DTU Library

Comparison of Reconfigurable BESS and Direct Grid Installation for EV Fast Chargers: a Danish Case Study

Calearo, Lisa; Engelhardt, Jan; Marinelli, Mattia; Agostini, Marco; Coppo, Massimiliano ; Turri, Roberto

Comparison of Reconfigurable BESS and Direct Grid Installation for EV Fast-Chargers: a Danish Case Study

Lisa Calearo, Jan Engelhardt, Mattia Marinelli
Department of Wind and Energy Systems
Technical University of Denmark
Roskilde, Denmark
{lica; janen; matm}@dtu.dk

Marco Agostini, Massimiliano Coppo, Roberto Turri
Department of Electrical Engineering
Padova University
Padova, Italy
{marco.agostini.2; massimiliano.coppo}@unipd.it

Abstract—**Battery energy storage systems (BESSs) are known as a potential solution to integrate renewables and electric vehicle (EV) charging in the power system. This article compares the direct grid installation of ultra-fast chargers (UFCs) with a hybrid system inclusive of a reconfigurable BESS, a photovoltaic (PV) unit, two UFCs and a grid connection. The hybrid system is simulated with an optimization model, which reveals that the overall efficiency of the system plays a major role in determining the power grid exchange. Results show that the hybrid system can increase the local PV consumption while reducing the grid impact of EV charging. Based on yearly results, the hybrid system shows potential for further improving the utilization of the BESS and unlocking new revenue streams.**

Index Terms—**Electric vehicle, hybrid system, PV production, reconfigurable BESS, ultra-fast charger.**

I. INTRODUCTION

Thanks to their ability to provide flexibility, battery energy storage systems (BESSs) are identified as a potential solution to integrate renewable energy sources (RES) and electric vehicle (EV) charging in the power system. Different studies have investigated how this can be achieved while considering both RES production and fast charging of EVs. For example, Ref. [1] proposes a 50 kW DC fast charging station supported by a photovoltaic (PV) unit and a battery storage. Such a configuration ensures the fast charger to operate at a constant power rate, limiting the charging impact on the distribution grid. Similarly, Ref. [2] discusses a DC ultra-fast charger (UFC) station, with a maximum charging power of 300 kW, connected to a PV unit with grid-side bi-directional AC-DC converter to limit the grid impact of EV charging. Other studies focus more on the economy of such systems, including comparisons with standard solutions for EV fast charging and feasibility studies. For example, Ref. [3] compares the economics of a DC fast charging station directly connected to the grid with a system including the charging station coupled with PV plants and/or BESSs of various sizes. Here, it is shown that annual cost savings grow proportionally with the PV size, while a non-linear growth is observed as a function of the battery capacity increment. Ref. [4] shows that fast charging stations can be profitable, but spikes in power

demand remain. Thus, RES and BESSs can be used to mitigate such stations' grid impact, improving the system profitability while balancing the intermittent production through the grid connection.

However, BESS interconnection with DC components is mostly performed through DC/DC and DC/AC converters [5]. These introduce losses and costs that can otherwise be avoided if reconfigurable BESSs are considered [6]. In a reconfigurable battery, the cell topology is flexible and the connections among cells can be changed depending on the necessities during operation. This improves energy efficiency, reliability and life span of the battery, allowing for better tailoring of the battery size [7]. The direct coupling of a reconfigurable BESS with other DC components is relatively new [8] and, as such, it requires some investigations on how it can be operated to maximize the system benefit. The present article compares the direct grid installation of two UFCs with the installation of two UFCs coupled with a reconfigurable BESS, a PV unit, and a grid inverter. In the following, the direct installation is named *standard solution (SS)* and the second solution *hybrid system solution (HS)*. The main contributions of this paper can be summarized as follows. First, a techno-economic comparison of the two solutions is provided to limit the EV charging impact on the grid and increase the local PV consumption. Second, insights about the management of the reconfigurable battery, optimal operating point, and potentials are discussed.

The rest of the paper is structured as follows. Section II presents techno-economic information of the two systems considered in this article. In Section III we describe the optimization algorithm implemented to simulate HS. Section IV presents the case study, data, results, and a discussion and comparison of the solutions. Section V concludes the work.

II. METHODOLOGY

This section presents the two solutions, SS and HS, in techno-economic terms in Section II-A, followed by the parameters considered for comparison in Section II-B.

A. Systems topology

UFCs are usually installed in commercial and industrial settings, where a private or a public entity pays for components and installation. Two main costs are to consider for the initial investment of a direct installation of UFCs: grid connection fee and UFCs price. Grid investments are excluded in this analysis. Considering a $350\,\mathrm{kW}$ UFC with two outlets, load sharing up to $175\,\mathrm{kW}$ per vehicle with two EVs connected, the fixed cost amounts to approx. $150\,000\,€$ [9], with projection costs to 2030 of $80\,000\,€$ [10]. This price includes both the costs for the charge posts - including outlets, cables, interface, and network connection - and the power cabinets - with power electronics. The grid connection fee in Denmark is about $150\,€/\mathrm{A}$ [11], which amounts to $75\,000\,€$ for a $350\,\mathrm{kW}$ charger with $500\,\mathrm{A}$ current rating [9]. The SS total cost is approx. $225\,000\,€$.

The SS is compared in this article with the HS introduced in Section I. The prototype of HS is today installed in Denmark in the parking lot of a school equipped with a PV plant [12]. The comparison of the two solutions is made from the grid perspective, where both systems are considered to be linked to the school consumption and PV production. Fig. 1 shows the systems topology: on the left SS with school, PV unit and grid; on the right HS integrated with one third of the PV unit, whereas school and remaining PV are unchanged. The operating principle of HS is to ensure that PV production is used first to charge EVs and second to export PV production to the school or the grid. The PV production cannot directly charge the EVs because the voltage of the two components is different. The HS price [12] or similar products on the market are not publicly available. Therefore, in the following, we estimated the price, which is comparable to the initial investment of the SS. The production cost of Li-ion battery price ranges between $150\text{-}200\,€/\mathrm{kWh}$ [13]. However, accounting for price variations, difference between battery producer and customer price, and technology value, the price is here considered to be $500\,€/\mathrm{kWh}$ [14]. For the considered BESS with $312\,\mathrm{kWh}$ ($104\,\mathrm{kWh}$ per string), the total price amounts to $156\,000\,€$. Additional costs are: grid connection fee, which in this work amounts to $9450\,€$ given a $43\,\mathrm{kW}$ grid connection ($63\,\mathrm{A}$); inverter price, in this case it is a $66\,\mathrm{kW}$ inverter ($\mathrm{Inv}_{\mathrm{HS}}$) with a price of about $10\,000\,€$; HS installation costs of about $10\,000\,€$. The total price amounts to $185\,450\,€$. Therefore, accordingly to price variations, the two solutions are considered to have a similar initial investment cost. The above prices do not include VAT.

B. Comparison parameters

To compare the two systems in techno-economic terms, three revenues/savings are considered: 1. revenue from charging EVs; 2. revenue from energy export (from PV production); 3. savings from local PV self-sufficiency increase. The comparison is done at the point of common coupling (PCC) by considering the following parameters: self-sufficiency, operating costs, and number of cycles. Self-sufficiency is defined as the ratio of consumed energy provided by local production and
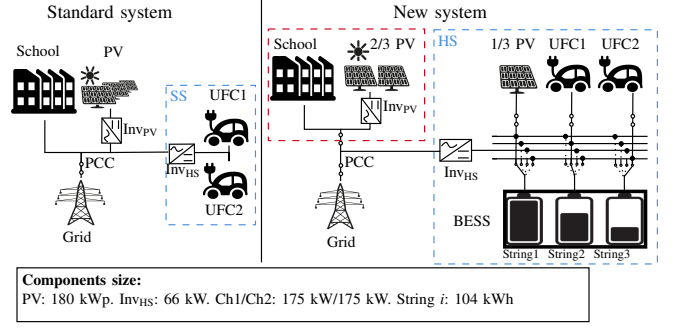

Fig. 1: Comparison of the two solutions connected to the remaining system.

Components size:
PV: 180 kWp. $\mathrm{Inv}_{\mathrm{HS}}$: 66 kW. Ch1/Ch2: 175 kW/175 kW. String i: 104 kWh

total consumption [15]. The operating costs (Cost) are the sum of revenue from energy sold to the grid and UFCs and costs from purchased energy. These are derived as in (1), accounting for energy imported (Import), exported (Export), and UFCs charged during a period T, where $t \in T$. $\Pi^{\mathrm{UFC1}}/\Pi^{\mathrm{UFC2}}$ are the power profiles of ultra-fast charger 1 (UFC1) and ultra-fast charger 2 (UFC2), and η is the $94\,\%$ charger efficiency [9]. c^{UFC} is the charging price per kWh, c^{i} and c^{e} are the import/export electricity prices per kWh.

$$\mathrm{Cost}_{\mathrm{SS}} = \sum_{t \in T} \left(c_t^{\mathrm{i}}\mathrm{Import}_t - c_t^{\mathrm{e}}\mathrm{Export}_t - c_t^{\mathrm{UFC}}(\Pi_t^{\mathrm{UFC1}}/\eta + \Pi_t^{\mathrm{UFC2}}/\eta)\right)\Delta t \quad (1)$$

In HS, $1/3$ of the PV is devoted to the HS. Assuming that the PV panels equally contribute to export and self-consumption, this causes a reduction of $33\,\%$ of the exported energy and of self-consumed energy from the school. This effect is taken into account in the $\mathrm{Cost}^{\mathrm{in}}$ in (3), where import is increased by $1/3$ of the school load and export is decreased to $2/3$ of the original value. Therefore, in HS costs are determined as sum of $\mathrm{Cost}^{\mathrm{in}}$ in the red square (see Fig. 1) and in the blue square ($\mathrm{Cost}_{\mathrm{HS}}^{\mathrm{Obj}}$):

$$\mathrm{Cost}_{\mathrm{HS}} = \mathrm{Cost}^{\mathrm{in}} + \mathrm{Cost}_{\mathrm{HS}}^{\mathrm{Obj}} \quad (2)$$

$$\mathrm{Cost}^{\mathrm{in}} = \sum_{t \in T} \left(c_t^{\mathrm{i}}\left(\mathrm{Import}_t + \frac{1}{3}\mathrm{School}_t\right) - c_t^{\mathrm{e}}\frac{2}{3}\mathrm{Export}_t\right)\Delta t \quad (3)$$

$\mathrm{Cost}_{\mathrm{HS}}^{\mathrm{Obj}}$ are derived with an optimization algorithm as in Section III, where HS is also used to compensate for the net school consumption (P^{Sc}).

Finally, the number of cycles is derived as the sum of charging/discharging string power divided by two times the string capacity.

III. HYBRID SYSTEM MODEL FORMULATION

This section summarizes the optimization model of HS, formulated as a day-ahead unit commitment problem and implemented as a mixed integer linear programming problem (MILP) in Matlab using YALMIP and Gurobi as solver. The model is solved for $24\,\mathrm{h}$ duration with timestep of $15\,\mathrm{min}$ (i.e. 0.25 hours). Formulas are reported for a generic instant $t \in T$. PV, BESS and inverter are modelled with active sign convention, while UFCs are modelled with passive sign convention. We refer to a string with the letter $i \in I$, where I is the number of strings.

1) Objective function: The objective function (4) minimizes the operating costs over the considered period. It consists of power exchanged with the grid at the AC side of Inv_{HS} ($P_t^{\text{giAC/geAC}}$, import and export respectively), and with UFCs ($P_t^{\text{UFC1/UFC2}}$). Exported power is the sum of P_t^{grid}, power sold to the grid, and P_t^{Sc}, power consumed by the school. This distinction is done because the power going from Inv_{HS} to the school has a different price than the export. Indeed, when the school self-consumes (from HS) the subsequent saving is equal to the avoided imported energy, hence $c_t^{\text{eSc}} = c_t^{\text{i}}$. The export grid price c_t^{e} is equal to the market one. c_t^{Ch} is the EV charging price.

$$\min_{P^{\text{giAC}}, P^{\text{grid}}, P^{\text{Sc}}} \quad \text{Cost}_{\text{HS}}^{\text{Obj}} = \sum_{t \in T} \Big(P_t^{\text{giAC}} c_t^{\text{i}} + P_t^{\text{grid}} c_t^{\text{e}} + P_t^{\text{Sc}} c_t^{\text{eSc}} \\ - (P_t^{\text{UFC1}} + P_t^{\text{UFC2}}) c_t^{\text{Ch}} \Big) \Delta t \tag{4}$$

The objective function is subject to the constraints described in the following subsections. The simulation has a Δt step time defined in hours, thus each power value is multiplied per Δt to obtain kWh.

2) Power balance constraint: To ensure the power balance, the sum of all powers at the DC side of Inv_{HS} is constrained to zero at each instant t:

$$P_t^{\text{UFC1}} + P_t^{\text{UFC2}} - P_t^{\text{PV}} - \sum_{i \in I}(P_{i,t}^{\text{bd}} + P_{i,t}^{\text{bc}}) - P_t^{\text{gi}} - P_t^{\text{ge}} = 0 \tag{5}$$

$P_{i,t}^{\text{bd}}$ is the string discharging power, $P_{i,t}^{\text{bc}}$ is the string charging power. $P_t^{\text{UFC1/UFC2}}$ is UFC1/UFC2 power and P_t^{PV} is PV power. $P_t^{\text{gi/ge}}$ is the power import/export at the DC side of Inv_{HS}.

3) Inverter constraints: The grid is the system slack, however the power exchanged is limited by the capacity of Inv_{HS}. Constraints (6) ensure that at each instant t there is import or export. The power exchange is bounded to the inverter capacity, by means of binary variables that are equal to 0 or 1.

$$P_t^{\text{g}} = P_t^{\text{gi}} + P_t^{\text{ge}}, \tag{6}$$

The inverter efficiency, function of P_t^{g}, links the power at AC and DC sides as in (7). In order to avoid non-linearity, the piecewise linear approximation is adopted to linearize (7) as proposed in [16].

$$P_t^{\text{giAC}} = P_t^{\text{gi}} / \eta_{\text{inv}}(P_t^{\text{g}}), \qquad P_t^{\text{geAC}} = P_t^{\text{ge}} \cdot \eta_{\text{inv}}(P_t^{\text{g}}), \tag{7a,b}$$

The power exported, sum of power flowing to the grid (P_t^{grid}) and to the school (P_t^{Sc}), is limited between 0 and the maximum power available for the grid and the school.

4) String power constraints: Each string can only do one action at a time t, charging ($P_{i,t}^{\text{bc}}$) or discharging ($P_{i,t}^{\text{bd}}$), within the charging/discharging power boundaries. Binary variables are used for the implementation.

Each string can charge from PV or grid, and can discharge by exporting to the grid, school, or UFCs (when an EV is connected). The string efficiency is function of charging/discharging power and it is implemented with N-piecewise linearization.

When switching a string from one component to another with a different voltage level, a time delay ($t_{\text{loss}} = 5sec$) is considered to avoid strong current transients. During this time there is no energy transfer. To keep a consistent model with Δt of 15 minutes, delay losses are spread equally over the entire time interval subsequent to the switching event. P_i^{bd} is the power including the connection loss, implemented as difference between expected power ($z_{i,t}^*$), and power switching loss ($w_{i,t}^*$).

In this investigation, the power produced and requested from PV, UFC1, and UFC2 is assumed a priori. Thus, the power switching loss ($w_{i,t}^{\text{PV/UFC1/UFC2}}$) represents a real power loss. Consequently, the string power is determined as difference between power profile $\Pi_t^{\text{UFC1/UFC2/PV}}$ and power switching loss ($w_t^{\text{UFC1/UFC2/PV}}$).

These constraints are implemented as in (8) for charging and (9) for discharging. Constraints (8)(b,c) are provided for a generic example, where $*$ indicates PV/gi/UFC1/UFC2/ge. All binary variables ($\beta_{i,t}^{*/*2}$) considered for implementation are fixed to be equal to 0 or 1. Also, to ensure that each string i at time t can do one and only one action, the sum of the binary variable $\beta_{i,t}^*$ is equal or smaller than 1.

$$P_{i,t}^{\text{bc}} = -(z_{i,t}^{\text{PV}} - w_{i,t}^{\text{PV}}) - (z_{i,t}^{\text{gi}} - w_{i,t}^{\text{gi}}) \tag{8a}$$

$$z_{i,t}^* = \beta_{i,t}^* \Pi_t^*, \quad w_{i,t}^* = \frac{t_{\text{loss}}}{\Delta t} \beta_{i,t}^{*2} \Pi_t^*, \tag{8b,c}$$

$$P_{i,t}^{\text{bd}} = (z_{i,t}^{\text{UFC1}} - w_{i,t}^{\text{UFC1}}) + (z_{i,t}^{\text{UFC2}} - w_{i,t}^{\text{UFC2}}) - (z_{i,t}^{\text{ge}} - w_{i,t}^{\text{ge}}), \tag{9}$$

Since the grid is the slack bus, the power import/export is a result of the optimization model. Therefore, the implementation as in (8)(b,c) results on the product between a binary and a continuous variable, which is linearized with the big-M formulation [17].

5) String energy constraints: The string energy $E_{i,t}$ is derived as difference between string energy at $t-1$ ($E_{i(t-1)}$) and charged/discharged power applied during Δt, see (10). Additionally, $E_{i,t}$ is constrained between maximum and minimum values at each instant t, and initial/final energy is fixed at a certain value (50 % of the capacity) to make the simulation replicable over time.

$$E_{i,t} = E_{i(t-1)} - (P_{i(t-1)}^{\text{bc}\eta} + P_{i(t-1)}^{\text{bd}\eta}) \Delta t, \tag{10}$$

6) BESS constraints: PV and UFCs are always prioritized. When the power profile of PV/UFC1/UFC2 ($\Pi_t^{\text{PV/UCF1/UCF2}}$) is different from zero, a string has to be available to absorb or inject power. This is implemented as follows

$$\begin{cases} \sum_{i \in I} \beta_{i,t}^{\text{PV/UFC1/UFC2}} = 0, \text{ if } \Pi_t^{\text{PV/UFC1/UFC2}} = 0 \\ \sum_{i \in I} \beta_{i,t}^{\text{PV/UFC1/UFC2}} = 1, \text{ otherwise} \end{cases} \tag{11}$$

Additionally, one and only one string can be connected to Inv_{HS} at each instant t, thus the sum of binary variables $\beta_{i,t}^{\text{gi/ge}}$ is equal to 0 or 1.

IV. Results

In this section, the two systems presented in Section II-A are compared. First, PV, school, and UFCs data are presented together with one-day results of SS in Section IV-A. Second, Section IV-B presents the operation of HS. Finally, Section IV-C compares the two solutions in techno-economic terms.

A. Standard solution

Fig. 2 shows the power profiles considered in this analysis and the resulting grid power import/export with the SS. In subplots (a) and (b), the (entire) PV production, school consumption and UFCs profiles are shown for two representative working days, one during summer (Wed, 24-Jun-2020) and one during winter (Wed, 15-Jan-2020). UFCs data are not available, thus fictitious profiles are considered by accounting that UFCs are located in front of a school. UFC1 charges 6 vehicles for $15\,\mathrm{min}$, 4 in the morning and 2 in the afternoon, and UFC2 charges 1 vehicle for $30\,\mathrm{min}$ in the morning. Considering the most common power charging level accepted from EVs today on the road, three charging events are considered with $100\,\mathrm{kW}$ and the remaining $50\,\mathrm{kW}$. Different charging profiles will be investigated in future studies, also strengthened by real measurements from the system [18]. Subplots (c) and (d) show the resulting import/export grid power profiles at the PCC. These are obtained from net metering PV production, school and chargers consumption.
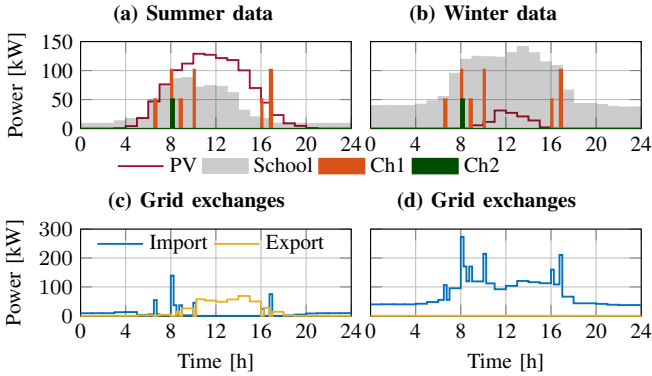
Fig. 2: (a)-(b) show PV production and school and UFCs consumption; (c)-(d) show import/export grid power profiles with the SS. (a)-(c) show summer profiles, (b)-(d) winter profiles. All quantities are displayed with positive signs.

B. Hybrid system solution

1) Power profiles: Fig. 3 shows the operation of HS in the summer and winter days considered. The strings absorb and deliver the requested production from PV and consumption from UFCs, while the exported power is split between school and grid. The optimizer prioritizes the school, due to the higher export electricity price. However, if summer PV production is enough to charge EVs and partially support the school, in winter the PV production is not sufficient for the UFCs energy request, and energy is also imported from the grid.
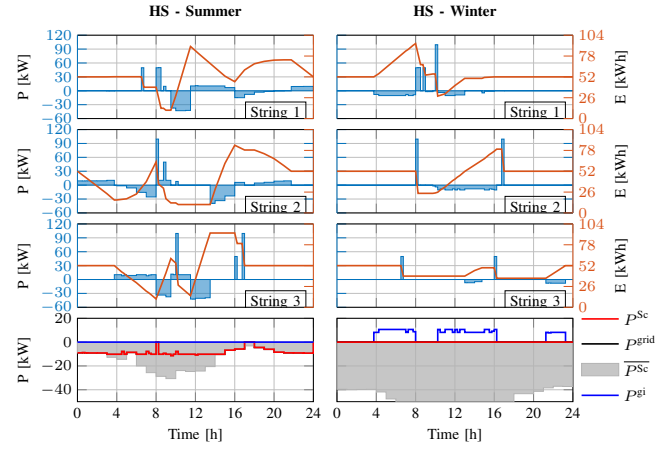
Fig. 3: HS: the first three rows show power (on the left axes) and energy (on the right axes) of the strings during summer (first column) and winter (second column) days. String charging power is negative, discharging is positive. The fourth rows show the exported power to the grid, divided between grid and school. Net school load and exported power are negative, import is positive.

2) Optimal operating point: During winter, whenever the system imports from the grid the power tends to stabilize around $8\,\mathrm{kW}$. This is due to the HS efficiency (η_{HS}) that is a combination of the inverter (η_{inv}) and string (η_i) efficiencies, as shown in Fig. 4.
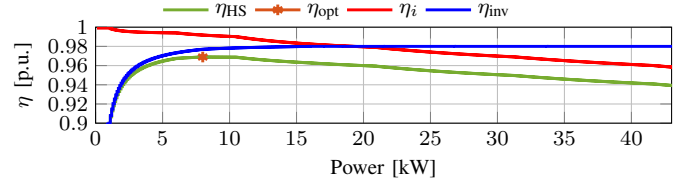
Fig. 4: Inverter, string, overall system, and optimal operating efficiencies.

The optimal operating efficiency (η_{opt}) is at $8\,\mathrm{kW}$. In the summer case, the power exported to the school is deviating from the optimal value, reaching $4.5\,\mathrm{kW}$ and $10.2\,\mathrm{kW}$. This is because following the school demand profile results in higher savings than continue exporting with the optimal operating efficiency.

C. Comparison and discussion

Table I compares the techno-economic results of the two solutions for the summer and winter days. In summer, the self-sufficiency increases from $77\,\%$ in SS to $89\,\%$ in HS, thanks to the compensation for the net school load that decreases the need for importing from the grid. In winter results are similar because the limited PV production nullifies the benefits of HS.

Due to the amount of binary variables necessary for the model implementation, an online utilization of the optimization algorithm is heavy to simulate. Thus, the model is here considered to provide the first steps for a long term techno-economic comparison of the two solutions, considering typical days. In this early analysis, two Sundays (19-Jan-2020 and 28-Jun-2020) are considered to better represent non-working days. Together with the summer and winter week-days previously

TABLE I: One-day techno-economic comparison of the two solutions.

	Summer		Winter	
	SS	HS	SS	HS
PV production [kWh]	1108		113	
School consumption [kWh]	790		1824	
EV charged energy [kWh]	137		137	
Imported energy [kWh]	211	132	1856	1863
Exported energy [kWh]	384	283	0	0
Self-sufficiency [%]	77.4	89.1	5.7	5.7
$\text{Cost}_{\text{HS}}^{\text{in}}$ [€]	-	75.0	-	437
$\text{Cost}_{\text{SS/HS}}$ [€]	-31.2	-44.0	391.5	397.4
Cycles Strings	-	1.03/1.17/1.24	-	0.64/0.53/0.25

presented, the annual behaviour is reproduced. As a conservative assumption and considering that the chargers are located close to a school, no vehicles are charged during Sundays and holidays. Table II summarizes seasonal and annual operating costs and battery cycles. HS is more profitable in summer than SS, whereas in winter the solutions are similar due to the need of importing energy from the grid to charge the vehicles. In terms of lifetime, the considered BESS has a cycle life of 6000 [19]. With the considered battery usage, the annual number of cycles is 257, corresponding to 23 years of lifetime when only considering cycle aging. When considering also the calendar aging, the battery lifetime would be reduced. However, this shows that in technical terms the BESS can be exploited at a deeper rate, which would also open new revenue potentials, e.g., more charging events, frequency regulation. Considering the solutions to have a comparable initial investment cost, yearly results show that the new system has economic potential, which will be further investigated in future work by considering deeper battery utilization. Also, uncertainties of power profiles and comparison with heuristic control strategies will be analyzed.

TABLE II: Daily, seasonal, and annual operating costs and strings cycles in SS and HS.

	SS				HS			
	Summer		*Winter*		*Summer*		*Winter*	
	Wed	Sun	Wed	Sun	Wed	Sun	Wed	Sun
Daily operating cost [€]	-31.2	-1.6	391.5	230.7	-44.0	-18.1	397.4	230.9
Seasonal operating cost [€]	-4057		62635		-6593		63401	
Annual operating cost [€]	58578				56808			
Seasonal average cycles	-		-		193.1		64.1	
Annual average cycles	-				257.2			

V. Conclusion

This article compares the direct connection of UFCs to the grid with the UFCs coupled with a reconfigurable BESS, a PV unit, and a reduced grid connection (HS). The two solutions are considered to have a similar initial investment. However, with the BESS in HS, energy can be moved over time, increasing the value of the PV unit and reducing the grid impact of UFCs. The power exchanged with the grid is found to be highly dependent on the system efficiency. Being the optimal operating point lower than the grid-tie inverter size, the power exchanged with the grid is reduced in comparison to the available power connection. On the one hand, this shows that HS can give the possibility to decrease the grid power connection and related costs. On the other hand, the BESS utilization capabilities should be further investigated by considering various EV, PV, school profiles and grid services, which can reduce the battery lifetime but also unlock new revenue streams.

References

[1] A. Sharma and R. Gupta, "PV-Battery Supported Level-1 DC Fast charger for Electric Vehicles," *2019 IEEE Students Conference on Engineering and Systems, SCES 2019*, pp. 1–5, 2019.

[2] Y. Liu and *et al*, "Fuzzy control based power flow control strategy of EV DC fast charging station including distributed PV generation and hybrid energy storage systems," *IET Conference Publications*, vol. 2019, no. CP764, pp. 1–8, 2019.

[3] L. Yang and H. Ribberink, "Investigation of the potential to improve DC fast charging station economics by integrating photovoltaic power generation and/or local battery energy storage system," *Energy*, vol. 167, pp. 246–259, 2019.

[4] J. A. Domínguez-Navarro and *et al*, "Design of an electric vehicle fast-charging station with integration of renewable energy and storage systems," *International Journal of Electrical Power and Energy Systems*, vol. 105, no. August 2018, pp. 46–58, 2019.

[5] M. A. H. Rafi and J. Bauman, "A Comprehensive Review of DC Fast-Charging Stations with Energy Storage: Architectures, Power Converters, and Analysis," *IEEE Transactions on Transportation Electrification*, vol. 7, no. 2, pp. 345–368, 2021.

[6] J. Engelhardt and *et al*, "Reconfigurable Stationary Battery with Adaptive Cell Switching for Electric Vehicle Fast-Charging," *UPEC 55th International Universities Power Engineering Conference, Proceedings*, 2020.

[7] N. Lin and *et al*, "An optimization framework for dynamically reconfigurable battery systems," *IEEE Transactions on Energy Conversion*, vol. 33, no. 4, pp. 1669–1676, 2018.

[8] J. Engelhardt and *et al*, "Double-string battery system with reconfigurable cell topology operated as a fast charging station for electric vehicles," *Energies*, vol. 14, no. 9, 2021.

[9] Electric Vehicle Infrastructure Terra HP high power charging. Available online: https://chargingshop.eu/wp-content/uploads/2020/06/ABB-Terra-HPC-Broshure.pdf.

[10] European EV Charging Infrastructure Masterplan. Research Whitepaper, March 2022.

[11] Trefor elnet. Tilslutningsbidrag. Available online. https://www.trefor.dk/elnet/priser/tilslutningsbidrag/. Accessed 05/2022.

[12] T. Gabderakhmanova and *et al*, "Demonstrations of DC Microgrid and Virtual Power Plant Technologies on the Danish Island of Bornholm," *UPEC 55th International Universities Power Engineering Conference, Proceedings*, 2020.

[13] Statista 2022. Lithium-ion battery pack costs worldwide between 2011 and 2030. Available: https://www.statista.com/statistics/883118/global-lithium-ion-battery-pack-costs/. Accessed 05/2022.

[14] Tesla. https://www.tesla.com/megapack/design. Accessed 05/2022.

[15] C. Ziras, L. Calearo, and M. Marinelli, "The effect of net metering methods on prosumer energy settlements," *Sustainable Energy, Grids and Networks*, vol. 27, p. 100519, 2021.

[16] W. Huang and *et al*, "Matrix modeling of energy hub with variable energy efficiencies," *International Journal of Electrical Power and Energy Systems*, vol. 119, no. January, p. 105876, 2020.

[17] J. Fortuny-Amat and B. McCarl, "A representation and economic interpretation of a two-level programming problem," *Journal of the Operational Research Society*, vol. 32, no. 9, pp. 783–792, 1981.

[18] INSULAE2020 project, Available online: http://insulae-h2020.eu/. Accessed 05/2022.

[19] Nerve Smart System. Battery datasheet. https://nervesmartsystems.com/.